Poster: mmWave CSI-based Sensing: a Feasibility Study

Joana Angjo*
angjo@ccs-labs.org
TU Berlin
Berlin, Germany

Falko Dressler
dressler@ccs-labs.org
TU Berlin
Berlin, Germany

Elena Tonini*
elena.tonini@unibs.it
University of Brescia
Brescia, Italy

Renato Lo Cigno
renato.locigno@unibs.it
University of Brescia
Brescia, Italy

ABSTRACT

Channel state information (CSI) is widely used for joint communication and sensing in sub-6 GHz wireless networks, but its application at mmWave frequencies remains underexplored. This work applies a quantized amplitude-based CSI similarity metric to data from a 28 GHz indoor testbed, showing the feasibility of CSI-based ambient sensing in next-generation wireless networks.

CCS CONCEPTS

• **Networks → Wireless access networks**; **Wireless access points, base stations and infrastructure**.

KEYWORDS

Joint Communication and Sensing, mmWave, Channel State Information, Non-Reconfigurable Reflecting Surface

*J. Angjo and E. Tonini contributed equally to this work and are listed as co-first authors alphabetically.

1 INTRODUCTION

Joint communication and sensing (JCAS) is emerging as a foundational technique for next-generation Wi-Fi and upcoming beyond-5G cellular networks. The possibility of acquiring information about the surrounding environment in parallel to communication has drawn the attention of both academia and industry for years. By leveraging the channel state information (CSI) extracted from a receiver, it is possible to capture the "electromagnetic footprint" that the propagation environment embeds within the signal [4]. Through Wi-Fi CSI analysis, recent deep learning (DL)-based approaches yield impressive results in performing passive localization [3] and activity recognition tasks [1].

However, as the demand for faster and energy-efficient wireless communication keeps rising, newer technologies than traditional sub-6 GHz telecommunication networks are being targeted: the attention has shifted to mmWave communications, which are the object of feasibility and resilience studies in real-world applications [5]. Integrating the CSI-based JCAS approach with mmWave communications can lead to high-resolution ambient sensing, while also enabling high-speed, directional communications, laying the foundations for truly intelligent and adaptive wireless networks.

2 CSI PROCESSING ALGORITHM

Building on the framework suggested in [2], this work extends the application of the quantitative analysis of Wi-Fi CSI to CSI samples collected in a communication system operating at 28 GHz. The goal is to be able to discriminate scenarios (e.g., empty room, one person standing still, one person walking) based on a quantitative analysis of CSI amplitudes. One CSI sample is extracted from each received packet. It represents channel distortion measured at the receiver: $\mathbf{C}(n) = A_{\mathbf{C}}(n)e^{j\angle \mathbf{C}(n)}$ where $n \in \text{SC} = [\frac{-N_{\text{SC}}}{2}, \frac{N_{\text{SC}}}{2} - 1]$ is the subcarrier index of the orthogonal frequency division multiplexing (OFDM) modulation. In a collection of $M_{\mathbf{C}}$
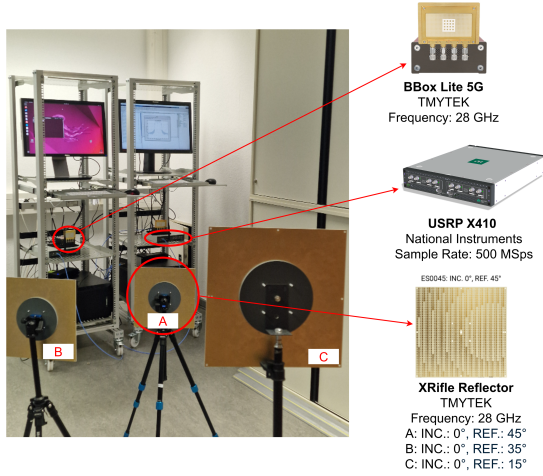
Figure 1: Testbed at 28 GHz.

CSI samples spanning over N_{SC} subcarriers, we compute the global maximum and minimum amplitude value and use them to map all CSI amplitudes onto the $[0, 1]$ interval. All A_C are then quantized using $q_{amp} = 9$ bits, representing them as a vector of N_{SC} integer values. Given two CSIs with the same number of subcarriers, we can compute the normalized distance between any two quantized samples $\mathbf{C_i}$ and $\mathbf{C_j}$ as:

$$W_D(A_{C_i}, A_{C_j}) = \frac{1}{N_{SC}(2^{q_{amp}} - 1)} \sum_{n \in SC} |A_{C_i}(n) - A_{C_j}(n)| \quad (1)$$

To keep a straightforward approach, we take the average of the CSI amplitudes collected for each experiment as the representative CSI of the collection:

$$A_C^\star(n) = \frac{1}{M_C} \sum_{k=1}^{M_C} A_C(k, n) \quad (2)$$

Finally, the similarity between two experiments i and j can be estimated by the distribution of distances W_D between the average of one experiment and all the CSI or the other:

$$W_D(A_{C_i}, A_{C_j}^\star); \quad \forall n \in [1, M_{C_i}] \quad (3)$$

3 EXPERIMENTAL SETUP

To analyze the algorithm's feasibility in mmWave frequencies, we set up an indoor testbed in our laboratory at TU Berlin (cf. Fig. 1). The testbed operating at 28 GHz features a reflector-assisted communication system. The hardware used for the setup includes the following components:

- **Software-defined radios (SDRs):** Two universal software radio peripherals (USRPs) X410 units (National Instruments) operating with a 500 MHz master clock rate, used for over-the-air communication.

Table 1: Number of CSI samples collected for each experimental scenario.

	LoS	1 reflector	2 reflectors	3 reflectors
# CSI	422469	337454	487103	344074

- **Clock distribution:** One OctoClock CDA-2990 (National Instruments) providing high-accuracy time and frequency references to synchronize the USRPs.
- **mmWave frontends:** Two BBox Lite 5G modules (TMYTEK) operating at 28 GHz with a 3 dB beamwidth.
- **Frequency conversion:** One UD Box 5G (TMYTEK) for up/down-conversion between IF and 28 GHz RF.
- **Passive reflecting surfaces:** Up to three ($\mathcal{N} = 3$) XRifle units (TMYTEK), passive non-reconfigurable reflecting surfaces (NRRSs) featuring 51×51 element arrays, operating at 28 GHz with a radar cross-section gain of approximately 70 dB.
- **Host machines:** Two PCs with AMD Ryzen 9 7950X 16-core CPUs, 128 GB RAM, and 100 GbE interfaces.

On the software side, the MATLAB WLAN Toolbox is used to generate an OFDM waveform with a 320 MHz bandwidth, compliant with the IEEE 802.11be standard. The transmitter continuously loops the generated waveform, while the receiver captures the signal for a duration of 10 seconds. We conduct a total of four main experiments. In the first set, $\mathcal{N} = 0$, meaning that communication occurs solely via the line-of-sight (LoS) path; the antennas shown in Fig. 1 are positioned facing each other with their beams properly aligned. In the subsequent experiments, we gradually increase the number of reflecting surfaces, i.e., $\mathcal{N} = 1, 2, 3$.

Before introducing the conducted experiments, it is important to note the working principles of NRRSs. Each NRRS reflects incoming signals at a fixed angle, with pre-configured incidence and reflection directions. In the experiments, we choose three NRRSs with an incident (INC) angle of $0°$ and reflection (REF) angles of $45°$, $30°$, and $15°$, respectively, to create strong additional signal paths between the transmitter and receiver. For each setup, traces are collected under different conditions: an empty lab room, a person sitting or standing still, and a person moving around the room.

4 RESULTS

The amount of data collected in the environment described in Sect. 3 is summarized in Tab. 1. Since the number of reflectors is the key feature of the experimental setup, computing the distance between two experiments performed with different values of $\mathcal{N}$ is meaningless. A different number of NRRSs completely alters the structure of the environment from a signal propagation point of view; therefore, CSIs collected with different $\mathcal{N}$ are 'semantically' incomparable.

(Exp. Setup 1) Line of sight (LoS), $\mathcal{N} = 0$

(Exp. Setup 2) One reflector, $\mathcal{N} = 1$

(Exp. Setup 3) Two reflectors, $\mathcal{N} = 2$

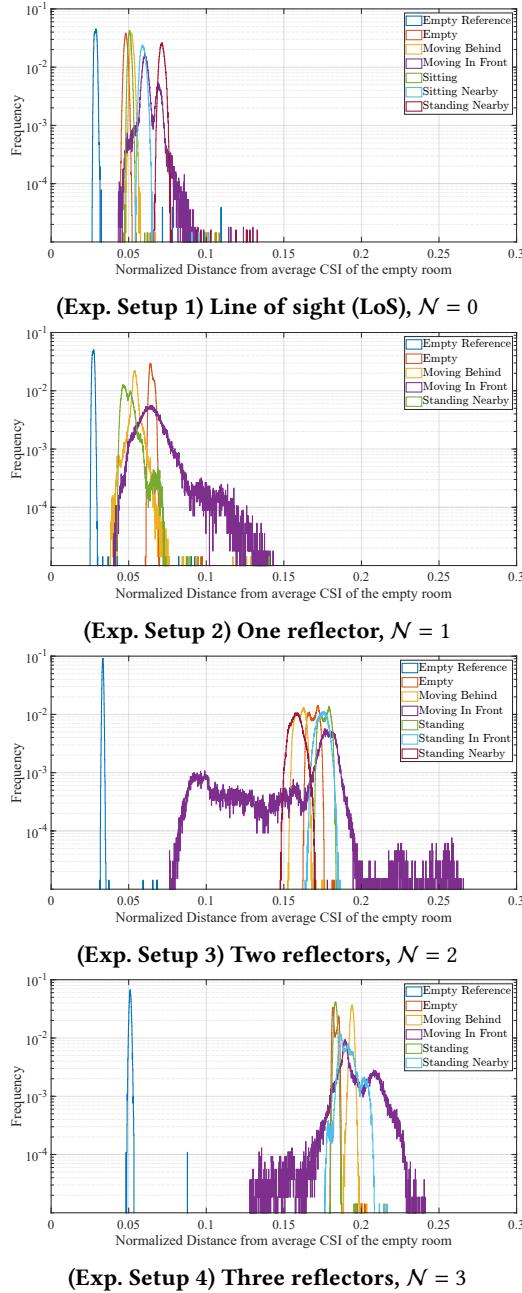**(Exp. Setup 4) Three reflectors, $\mathcal{N} = 3$**

Figure 2: Distributions of the normalized distance from the average CSI of the reference Empty Room.

For each number of reflectors ($\mathcal{N} = 0 \ldots 3$), we select a reference experiment, A^R, performed in the Empty Room from which to compute the distance distribution of all the experiments. For all available experiments, including A^R, we compute $W_D(A_C^i, A_C^{R\star})$ (Eq. (3)). For A^R, this corresponds to the distance from its own average CSI, for all other captures, we evaluate the distance from the average CSI of A^R.

The distributions of W_D showcased in Fig. 2 highlight a significant similarity of A^R with its $A_C^{R\star}$, with W_D values distinctly lower than the distances from the other experiments. This behavior indicates how the CSI's collected in the Empty Room are very similar to each other, implying that a perfectly static environment does not cause relevant variations of CSI amplitude. Regardless of $\mathcal{N}$, a person moving between the reflectors and the receiver causes significant modifications to A_C, which in turn results in a greater distance from $A_C^{R\star}$. This outcome validates the intuition that the increased dynamism of the scenario leads to a more variable propagation channel.

5 CONCLUSION

This introductory study on mmWave CSI-based sensing demonstrates the applicability of a quantized amplitude-based CSI similarity metric – originally proposed for Wi-Fi CSI – to data collected on a system operating at 28 GHz. The presented results align with those observed in sub-6 GHz applications, suggesting that a more in-depth analysis could yield a promising outcome.

REFERENCES

[1] Zhengran He, Xixi Zhang, Yu Wang, Yun Lin, Guan Gui, and Haris Gacanin. 2023. A Robust CSI-Based Wi-Fi Passive Sensing Method Using Attention Mechanism Deep Learning. *IEEE Internet of Things Journal* 10, 19 (Oct. 2023), 17490–17499. https://doi.org/10.1109/jiot.2023.3275545

[2] Elena Tonini, Francesco Gringoli, Renato Lo Cigno, and Marco Cominelli. 2025. Towards a Quantitative Analysis of CSI for AI/ML Based Sensing. In *IEEE WCNC 2025*. IEEE, Milan, Italy, 1–6. https://doi.org/10.1109/wcnc61545.2025.10978183

[3] Xuyu Wang, Lingjun Gao, Shiwen Mao, and Santosh Pandey. 2017. CSI-based Fingerprinting for Indoor Localization: A Deep Learning Approach. *IEEE Transactions on Vehicular Technology* 66, 1 (March 2017), 763–776. https://doi.org/10.1109/TVT.2016.2545523

[4] Kaishun Wu, Jiang Xiao, Youwen Yi, Dihu Chen, Xiaonan Luo, and Lionel M. Ni. 2013. CSI-Based Indoor Localization. *IEEE Transactions on Parallel and Distributed Systems* 24, 7 (July 2013), 1300–1309. https://doi.org/10.1109/tpds.2012.214

[5] Anatolij Zubow, Joana Angjo, Sigrid Dimce, and Falko Dressler. 2025. Achieving Resilience in mmWave Communications by Using Non-reconfigurable Reflecting Surfaces. In *IEEE WCNC 2025*. IEEE, Milan, Italy, 1–6. https://doi.org/10.1109/WCNC61545.2025.10978566